Paper
Int'l J. of Aeronautical & Space Sci. 17(1), 64–72 (2016)
DOI: http://dx.doi.org/10.5139/IJASS.2016.17.1.64

IJASS
International Journal of Aeronautical and Space Sciences

Extending Ionospheric Correction Coverage Area By Using A Neural Network Method

Mingyu Kim* and Jeongrae Kim**

School of Aerospace and Mechanical Engineering, Korea Aerospace University, Goyang City, Gyeonggi-Do 10540, Republic of Korea

Abstract

The coverage area of a GNSS regional ionospheric delay model is mainly determined by the distribution of GNSS ground monitoring stations. Extrapolation of the ionospheric model data can extend the coverage area. An extrapolation algorithm, which combines observed ionospheric delay with the environmental parameters, is proposed. Neural network and least square regression algorithms are developed to utilize the combined input data. The bi-harmonic spline method is also tested for comparison. The IGS ionosphere map data is used to simulate the delays and to compute the extrapolation error statistics. The neural network method outperforms the other methods and demonstrates a high extrapolation accuracy. In order to determine the directional characteristics, the estimation error is classified into four direction components. The South extrapolation area yields the largest estimation error followed by North area, which yields the second-largest error.

Key words: GNSS, ionospheric delay, spatial extrapolation, neural network, biharmonic spline

1. Introduction

The positioning accuracy of a single frequency global navigation satellite system (GNSS) receiver is limited mainly due to ionospheric delay errors. An ionospheric map provides ionospheric correction data to minimize the ionospheric error. The international GNSS service (IGS) provides a global ionosphere map to correct the ionospheric error. Since the IGS Map is provided as a post-processed data, a regional ionospheric map is required for real-time use. An example to illustrate this is with the satellite-based augmentation system (SBAS) which generates a real-time ionospheric delay map. The coverage area of a regional ionospheric map is limited by its ground based infrastructure such as GNSS monitoring stations. In the case of South Korea, only a small coverage area is feasible due to the country's small ground area.

The ionospheric delay has a certain level of geographical correlation as well as a time correlation. For the geographical correlation part, the extrapolation of the ionospheric delays for outside the ionosphere map is feasible. The extrapolation can be used to overcome the coverage limitation. The ionosphere activity is highly correlated with seasonal and hourly variations, and these variations are directly correlated with the solar and geomagnetic activity. Using this information may improve the extrapolation's accuracy. Use of the solar/geomagnetic indices is related with the prediction of ionosphere activity. There have been a series of researches on using the solar and geomagnetic activities to predict ionospheric delays. Among prediction methodologies, neural network (NN) has been a primary tool to predict the variation. McKinnell and Friedric [1] applied the NN approach to predict the lower ionosphere in the aurora zone. Habarulema [2, 3] used the NN to predict total electron content (TEC) variation in South Africa. Solar/geomagnetic indices, day / hour numbers, and TEC observation locations are used for the input data of training process. El-naggar [4] also used NN for modeling TEC. He considered user's latitude, longitude, hour in day, and day number as the parameters of NN. In addition to NN, the empirical model or the other extrapolation method has been used to estimate the TEC. Wielgosz [5] interpolated

* Graduate student, Ph.D. program
** Professor, Corresponding author: jrkim@kau.ac.kr

Received: July 27, 2015 Revised: February 18, 2016 Accepted: February 24, 2016

http://ijass.org pISSN: 2093-274x eISSN: 2093-2480

and predicted the TEC maps by using Kriging and multi-quadratic model with GPS observations over a regional area. Opperman [6] used adjusted spherical harmonic model (ASHA) for near real-time regional ionospheric TEC mapping over South Africa.

In contrast to the temporal extrapolation of ionosphere, i.e. TEC prediction, researches on the spatial extrapolation of the ionosphere have been hardly performed. Habarulema [3] performed some spatial extrapolation of TEC outside the observation area by changing the location input data to the NN processing. Since most of extrapolation methods based on interpolation methods, Kim [7] applied three interpolation methods to extend the ionospheric correction coverage area of South Korea. Krigging, cubic spline, and bi-harmonic spline (BHS) methods were evaluated, and the BHS method clearly outperforms the other two methods. An 81% of error reduction is achieved in comparison with the GPS broadcast ionospheric corrections. These methods utilized observation data only, and extrapolated the data epoch-by-epoch. Neither solar nor geomagnetic data was used.

We propose a new ionospheric delay extrapolation method by combining the solar/geomagnetic indices with the spatial extrapolation. As an extrapolation method, the NN is selected because the NN has a good generalization performance. Especially, the optimal prediction can be realized with the input similar to the training model. A NN is trained to extrapolate the TEC outside the observation region. The observed TEC inside the region as well as the solar/geomagnetic indices are then used for the NN processing. Habarulema's method [3] does not utilize the TEC observation data as an input because additional error can be generated when the observed TEC is converted into the TEC map. Kim's method [7] also does not utilize the solar/geomagnetic indices and therefore a time correlation between the estimates is not considered. The proposed method utilizes both of the data sets. Extrapolation performance of ionospheric delay around South Korea is evaluated by applying the combined NN method. IGS global ionosphere map data is used to establish a truth value. Since IGS TEC map can be assumed to have no errors, our study analyzes only the extrapolation error. Eleven years' of IGS data set is used to train the NN processor. For comparison of performance, a least square regression (LSR) model is also tested.

2. Ionosphere Map Extrapolation

A grid-based ionosphere map may consist of TEC values at each grid point as

$$I_{obs} = \left[TEC_1 \quad TEC_2 \quad \cdots \quad TEC_N \right] \tag{1}$$

Where I_{obs} is an array of the TECs in observation area. TEC_i, i= 1, 2, ..., N is the TEC value in i-th observation area. The map consists of N data points. Those values are determined by processing the GNSS dual-frequency observations. The ionosphere map coverage can be extended by applying the extrapolation method to the ionosphere map data. An extrapolated map may consist of extrapolated TEC values at outside grid point as

$$I_{extp} = \left[eTEC_1 \quad eTEC_2 \quad \cdots \quad eTEC_M \right] \tag{2}$$

where I_{extp} is an array of the TECs in extrapolation area. $eTEC_j$, j= 1, 2, ..., M is TEC value in i-th extrapolation area. The number of extrapolated points is M. A pure spatial extrapolation method utilizes the observation TEC, I_{obs}, only and any other extra information is not required. The time correlation of the observation data is not considered, and neither are the correlation with environment parameters, e.g. solar index. An alternative approach can be a mixed use of both the observation TEC and the environment parameters. The NN or least square regression (LSR) method is well suited for this type of mixed data.

The extrapolated ionospheric delay can be represented as a function of the observed TEC and environment parameters as

$$eTEC_i = f\left(I_{obs}, \quad x_e \right) \tag{3}$$

where the set of environmental parameters are as follows:

$$x_e = \left[C_D, \quad S_D, \quad C_H, \quad S_H, \quad R, \quad Ap \right] \tag{4}$$

where C_D and S_D are cosine and sine of day number, respectively. C_H and S_H are cosine and sine of hour number, respectively. The ionospheric delay variation is highly correlated with hourly and seasonal variations, and the variation can be approximated with sinusoidal functions. For this reason, the sinusoidal functions of hourly and seasonal variations are as follows [2, 3]

$$C_D = cos\left(2\pi\omega_D t_D \right) \quad S_D = sin\left(2\pi\omega_D t_D \right) \tag{5}$$

$$C_H = cos\left(2\pi\omega_H t_H \right) \quad S_H = sin\left(2\pi\omega_H t_H \right) \tag{6}$$

where t_D is a day number ranging from 1 to 365 or 366 and ω_D is a daily variation frequency of 1/365.25. The hour number t_H ranges from 0 to 24 and ω_H is an hourly variation frequency of 1/24.

Since the solar activity directly affects the ionospheric delay, the Sun spot number, R, can be used for adopting this effect.

The Sun spot number does not have a continuous variation, and the epoch-by-epoch use of the Sun spot number is not appropriate for prediction. Instead the moving average of the number is adopted for this research. Selection of the moving window is discussed in section 4. Geomagnetic activity also affects the ionospheric delay, and the geomagnetic index can be considered as the environmental parameter. The Ap index, which quantifies the global geomagnetic storm, is considered as the environmental parameter. As like the Sun spot number, a moving averaged value is preferred to an epoch-by-epoch value.

Finding an optimal function f in eq. (3) is the main topic of this research. Coefficients of function f are calculated for each outside grid points with the same inputs, I_{obs} and x_e. Thus, the information of extrapolation positions is not considered as parameters.

3. Extrapolation Methods

Three methods are tested for the extrapolation function f of Eq. (3); BHS, LSR, and NN. The mathematical description of these methods is presented as follows.

3.1 Bi-Harmonic Spline (BHS)

As a pure spatial extrapolation method, the BHS is selected for experiment. Preliminary analysis comparing three spatial extrapolation methods [7] shows that the BHS method outperforms the other spatial extrapolation methods, Kriging and cubic spline. For this reason only the BHS is considered in this research. The BHS is a method of finding the minimum-curvature surface, which passes through a set of points [8]. For N data points in m dimensions the interpolation problem is [9]

$$\nabla^4 \omega(x) = \sum_{j=1}^{N} \alpha_j \delta(x - x_j) \tag{7}$$

$$\omega(x_i) = \omega_i \tag{8}$$

where ∇^4 is a biharmonic operator and δ is a dirac delta function. $\omega(x)$ is weight function, and $\omega(x_i)$ is weight of i-th position x_i. x is a position vector. The weight $\omega(x)$ can be represented as

$$\omega(x) = \sum_{j=1}^{N} \alpha_j \phi(x - x_j) \tag{9}$$

where $\phi(x)$ is a Green's function which is the impulse response of an inhomogeneous differential equation [10], and α_j is a weighting factor. A second order Green's function is

$$\phi(x) = |x|^2 \left(ln|x| - 1\right) \tag{10}$$

The factor α_j can be determined by minimizing the slope s_i as

$$s_i = \left(\nabla\omega \cdot n\right)_i = \sum_{j=1}^{N} \alpha_j \nabla\phi\left(x - x_j\right) \cdot n \tag{11}$$

where s_i is a unit vector in the direction n_i. The BHS method can be numerically unstable for large numbers of points and has a tendency to drastically overshoot when points are close together [8]. The BHS utilizes the observed TEC only and does not require the environmental parameters. Therefore, the extrapolation becomes the function of observed TEC only as follows

$$I_{extp} = f\left(I_{obs}\right) \tag{12}$$

3.2 Least-Square Regression (LSR)

In order to apply the environmental parameters as well as the observed TEC, the LSR is used to define the extrapolation function. We can assume that the input variables have a linear relationship with the following output variables;

$$y = H\boldsymbol{x} \tag{13}$$

where the output variable is the extrapolated TEC at i-th outside point as

$$y = \left(I_{extp}\right)_i \tag{14}$$

The input variable consists of the observed TECs and the environment variables:

$$x = \left[I_{obs} \quad x_e\right] \tag{15}$$

The mapping matrix H maps the input variables to the output variables. The least square equation can be rewritten with individual terms as follows

$$\begin{aligned}\left(\mathrm{I}_{\mathrm{extp}}\right)_i = {} & c_1 TEC_1 + c_2 TEC_2 + \cdots c_N TEC_N \\ & + c_{N+1} C_D + c_{N+2} S_D + c_{N+3} C_H + c_{N+4} S_H + c_{N+5} R + c_{N+6} Ap\end{aligned} \tag{16}$$

The LSR problem is to determine the set of coefficients c_i by fitting past data at the extrapolation area. Habarulema [3] tested the LSR to predict TEC variation, but the observed TEC values were not used for the LSR. Only the six coefficients from c_{N+1} to c_{N+6} were estimated.

3.3 Neural Network (NN)

The NN is a statistical learning model and has a similar structure to the biological neural network. A NN is composed of neurons and synapses, and neurons are interconnected

with synapses which store weights. A NN can solve the problem by changing the weights from the learning of the neurons [11, 12].

The back-propagation neural network (BPNN) is one of the most widely used NN's. It is a feed-forward, multi-layer perceptron (MLP), supervised learning network [13]. The feed-forward network maps sets of input onto a set of output data. A MLP consist of multiple layers, with each layer connected to the next one. In the Input-output mapping process, activation function or transfer functions are involved. The activation functions determine the activation of inputs from the previous layer. The supervised learning method consists of a learning task which infers a function from the training data when the input-output relationships are known or pre-defined [14]. Learning the NN is generally performed by computing a gradient descent, using back-propagation [3]. The BPNN is applied to define the function $f(I_{obs}, x_e)$.

Figure 1 illustrates the network architecture. All the N observed TEC and another 6 environmental parameters are mapped to one hidden and output layers. After the input-output and target of the network is set, weight are randomly initialized within the range of $-1 \le w \le 1$. The network output is calculated by combining each weight and activation function as

$$y_{net} = f^{n}\left(W^{n,n-1} f^{n-1}\left(W^{n-1,n-2} f^{n-2}\left(\cdots f^{1}\left(W^{1,0}u + b^{1}\right)\cdots + b^{n-2}\right) + b^{n-1}\right) + b^{n}\right) \quad (17)$$

where y_{net} is network output, f represents the activation function, n represents n-th layer, u represents the network inputs, and b represents network bias. $W^{n,\,n-1}$ represents the weight from layer n-1 to n. The hyperbolic tangent sigmoid function is one of the most widely used activation functions as [15]:

$$f(x) = \frac{2}{1+e^{-2x}} - 1 \quad (18)$$

Hyperbolic tangent sigmoid function is in the range of (-1, 1), and y is zero when x is zero. The network can be characterized as calculating the weights of a network such that the following mean squared error (MSE) is minimized:

$$e = \frac{\Sigma\left(y - y_{net}\right)^2}{N} \quad (19)$$

where e is MSE, y is the reference output or desired output, and N is number of data. The NN training is based on minimization of the MSE of reference output minus number of data as described in eq. (19). In the case of this paper, y is the TEC value outside the observation region.

The training stands for the process of updating and computing of the gradients of weights and biases. There are many types of training methods such that gradient descent method, Bayesian regularization, Levenberg-Marquardt method, etc [15]. In this paper, the Levenberg-Marquardt method is selected. In general, the network data is divided into three subsets: training, validation, and test set. The reason for dividing the network is in order to be able to reduce the memory used for the computation, as well as to avoid over-fitting. The training set is used for calculating the gradient and updating the network weights. The validation set is monitored during the training process to minimize over-fitting. A test set is used only for testing the final solution. In this paper, training, validation, and the test set is allocated to 70%, 15% and 15%, respectively. The difference from Habarulema's NN prediction method [3] is in the presence of the observation TECs. His NN prediction algorithm utilizes the environmental parameters only.

4. Data Processing

The extrapolation performance is dependent on the data characteristics, and it is important to use a realistic data for evaluating the extrapolation performance. IGS provides a

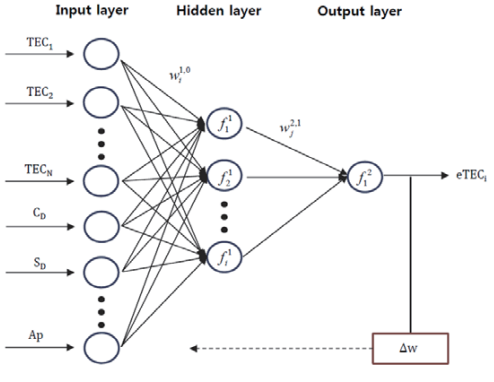

Fig. 1. Neural network architecture for ionosphere map extrapolation

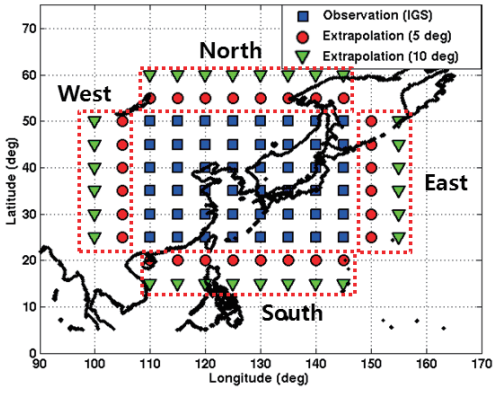

Fig. 2. Observation and estimation areas of ionospheric delay data

global ionosphere map by using globally distributed ground network data. Thanks to its large number of observations and advanced processing algorithms, it is reasonable to use the IGS map data as a truth value.

Figure 2 illustrates the observation data area (square) and the extrapolation data area (circle) near the Korean peninsula. The latitude of the observation area ranges from N25˚ to N50˚, and the longitude ranges from E110˚ to E145˚. The observation area is approximately close to the area where the GNSS satellites are visible at the center of Korea with a mask angle of 5˚. The grid size is 5˚ for both the latitude and longitude. The IGS map grid size is different for the latitude and longitude; 2.5˚ along the latitude and 5˚ along the longitude. For the other regional ionosphere maps, an equal grid size is generally used. For example, SBAS has a grid size of 5˚ along both the latitude and longitude. For general applications, an equal 5˚ grid size is used for the latitude and longitude directions in this research. The extrapolation area is set as two types; 5˚ and 10˚. Fig. 2 shows the 5° and 10° extrapolation area. In the case of the 5° extrapolation area, the latitude of the North and South extrapolation areas are 55° and 20°, respectively (longitude from 110° to 145°). The latitude of North and South direction and the longitude of East and West 10° extrapolation area are 5° extended from 5° extrapolation area. The number of observed TEC points is 54 and the number of extrapolated TEC points is 28.

The ionospheric delays at 5˚ or a 10˚ area are estimated every two hours by using both observation and environmental data. The ionospheric delay in 2014, when the geomagnetic index Ap was very high and the ionospheric variation was very high, is selected for this evaluation. Previous research [7] showed that the extrapolation during low geomagnetic activity, e.g. 2007, yielded a relatively low extrapolation error. In contrast the high ionospheric activity period yielded a high extrapolation error, and then this research focuses on the high activity period, 2014. The Solar sun spot number varies with an approximately 11 year cycles, and the ionospheric variation behavior repeats every 11 years. For training the LSR and NN processors, 11 years of data, which are solar/geomagnetic indices and TEC values inside and outside the observed region, from January 1, 2003 to December 31, 2013 are used. In the training process, the coefficients which mapping the TEC of the inside region and environmental parameters to the TEC of the outside region are calculated. It takes approximately two hours for training with 11 years data. Since the main purpose of this thesis is to demonstrate the feasibility of the TEC extrapolation using a NN, the post-processing NN method is used instead of a real-time NN method.

The NN prediction results depend on the number of hidden neurons. If the number of hidden neurons is too high, an overfitting problem occurs and it causes longer computation time. If the number of hidden neurons is too low, the problem becomes an ill-conditioned problem. Because there are no criteria for the range of hidden layer size, the layer size is determined empirically. By changing the layer size, the estimation errors are computed and compared. Based on these trial and errors, the number of hidden neurons is set to 80.

The length of the moving average windows for the Sun spot number R and the geomagnetic index are determined empirically as well. After a series of experiments were conducted by changing the window length, the moving average window for R is set to 7 months and the window for Ap is set to 8 hours.

5. Results

Three extrapolation methods, BHS, LSR, and NN, are tested for the evaluating the estimation accuracy. One-day data is analyzed to figure out the characteristics of each method, and then one-year data is analyzed to compute statistical values.

5.1 Single-day analysis

Extrapolation error characteristics on September 8, 2014 are analyzed. This date is selected because the geomagnetic activity on this date is close to the daily mean value and the 24 hour ionospheric variation is close to the overall variation.

Figure 3 illustrates the ionospheric delay distribution of East Asia at 6 universal time (UT) on Semptember 8, 2014. The local time is 15 Korea standard time (KST), and the ionospheric delay is close to its peak. In the South, the equatorial anomaly is passing and it causes a high

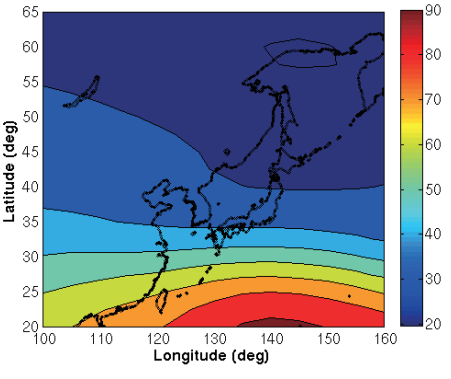

Fig. 3. Ionospheric delay distribution of East Asia (6UT, September 8, 2014, unit= TECU)

ionospheric delay in the South region. The North-South direction has a large ionospheric spatial gradient in the daytime while the East-West direction has a small gradient [16].

Figure 4 shows the TEC variation during a 24 hour period on September 8, 2014. This TEC value is labeled as 'signal' and plotted for each direction. The TEC values at the midpoint of each 5° extrapolation area is presented for every two hours. The midpoints of North, South, East, and West are (N55°, E125°), (N20°, E125°), (N40°, E105°), and (N40°, E150°), respectively. The TEC has a maximum value at 6 or 8 UT and has a minimum value around 20 UT. The South point shows the largest TEC and the North point shows the smallest TEC. The ionospheric delay computed from the GPS broadcast is presented for reference. The difference between the signal TEC and broadcast TEC represents the ionospheric model error of the broadcast model. The estimated TEC using extrapolation methods should provide better results than this broadcasted TEC.

Figure 5 compares the estimation errors using the three methods. One of the extrapolation points at the 5° area is selected for evaluation. The evaluation point is located at (N20°, E125°) which is the center of the South extrapolation area. Since the South area has the largest TEC values and the largest extrapolation error, this South point is selected for the evaluation. The extrapolated TEC value is subtracted from the true IGS TEC value in order to compute the estimation error. BHS yields the largest TEC error while NN yields the smallest TEC error. The RMS error is 13.88 TECU for BHS and 40.04 TECU for NN, respectively. The RMS error of the LSR error is 5.581 TECU, between the two methods. The maximum error occurs between 12 and 14 UT when the TEC level is decreasing from the peak at around 6 UT.

Figure 6 compares the estimation errors at the 10° extrapolation area. The center of the South 10° area is selected for evaluation. Similar to the results found at 5°, the NN shows the smallest error level. The BHS error reaches up to 25 TECU, and one can conclude that BHS is not appropriate for the 10° extrapolation area.

The estimation error depends on the TEC variation, and the ionospheric errors in each direction are presented in Fig. 7. The estimation errors by NN are plotted. The midpoint of each 5° extrapolation area is selected for evaluation. The South point yields the largest error. The North point yields the second largest error; larger than the East or West point. Considering the lowest TEC level in the North area, this error level is not expected because the extrapolation error is usually proportional to the TEC level. One of the possible causes of the relatively large error is the ionospheric spatial gradient. The North-South direction has a larger gradient than the East-West direction does. The gradient implies

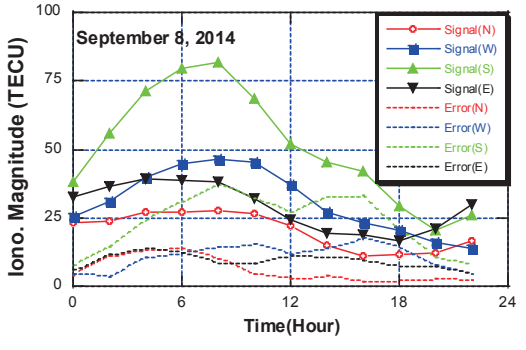

Fig. 4. Actual TEC and GPS broadcast error for each direction

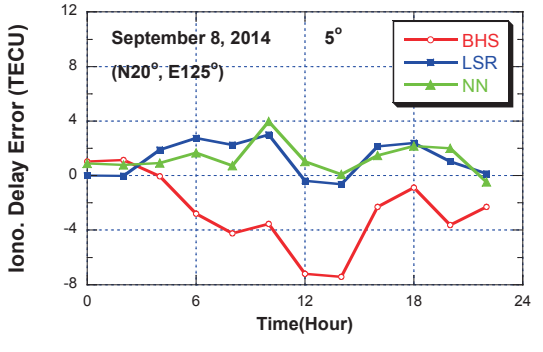

Fig. 5. Estimation error variation on September 8, 2014 (5° extension)

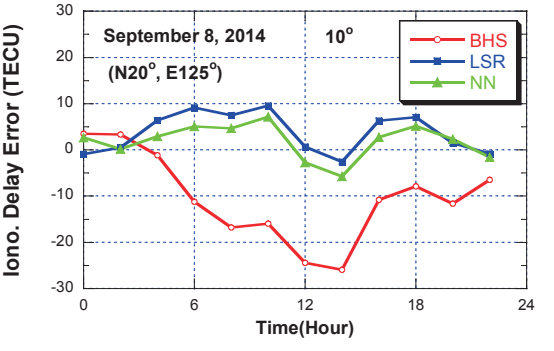

Fig. 6. Estimation error variation on September 8, 2014 (10° extension)

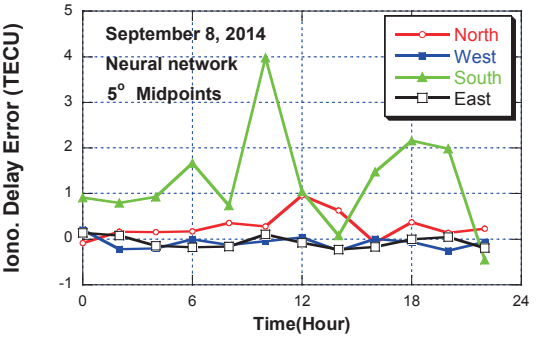

Fig. 7. Estimation error variation for each direction by the NN method (September 8, 2014, 5° extension)

a spatial difference and the large gradient magnifies the extrapolation error. Both the North and South points have positive errors, which imply the estimated TEC is larger than the true TEC.

5.2 One year analysis

One year of estimation error is analyzed by using the three methods. The estimation period is from January 1, 2014 to December 31, 2014. Similar to like the single-day analysis, 11 years of data from 2003 to 2011 are used for training the NN and LSR. Year 2014 is near the Solar maximum and its daily TEC level is higher than that of preceding years, close to 2003 when many severe ionosphere storms happened.

Figure 8 compares the daily estimation error variations at the South of the 5˚ extrapolation area in 2014. A midpoint at (N55˚, E125˚) is selected for computing the daily RMS errors. Similar to the single-day results, the NN outperforms the other two methods. The one-year averages of the RMS errors are 1.70 TECU for LSR, and 1.47TECU for NN, respectively. The difference between the BHS and the other methods becomes significant in Spring and Fall. This seasonal error variation corresponds to the seasonal TEC variation. During the high TEC period, the BHS error level is very proportional to the TEC level, and its error grows significantly.

Figure 9 shows the daily estimation error variation at the North of 5˚ extrapolation area in 2014. The overall error level and the difference between the BHS and the others are not significant at the North area. From these plots, one can conclude that the BHS error level depends on the signal (TEC) magnitude. Actually, in Fig. 10, the ionospheric delay is high at Spring and Autumn, but low at Summer and Winter. The variation of the true TEC value is similar to the BHS error variation. During high ionospheric delay periods, the BHS is not appropriate for the extrapolation, although it is still better than the GPS broadcast model.

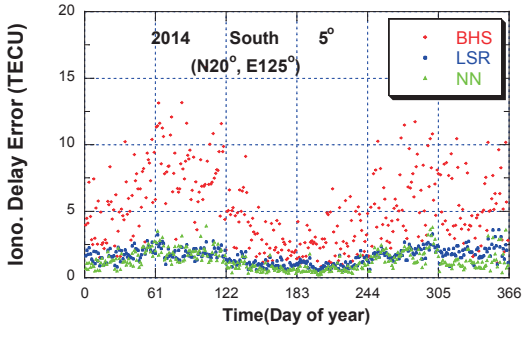

Fig. 8. Daily RMS error variation at the South midpoint in 2014 (5° extension)

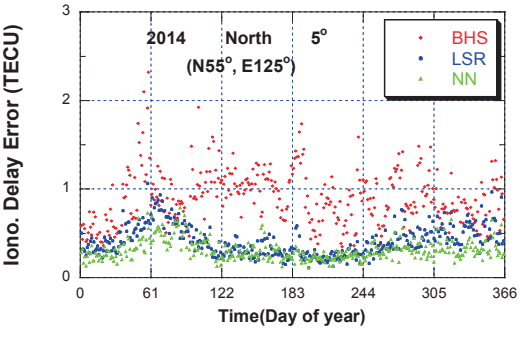

Fig. 9. Daily RMS error variation at the North midpoint in 2014 (5° extension)

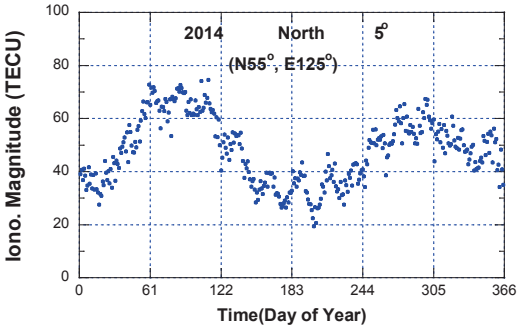

Fig. 10. Daily mean variation of IGS TEC map at the North midpoint in 2014 (5° extension)

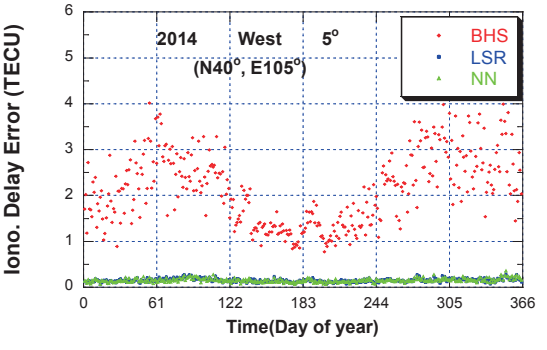

Fig. 11. Daily RMS error variation at the West midpoint in 2014 (5° extension)

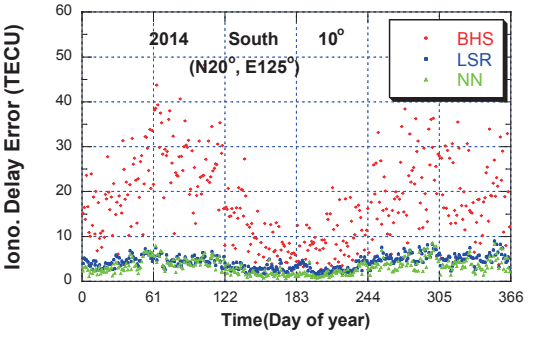

Fig. 12. Daily RMS error variation at the South midpoint in 2014 (10° extension)

DOI: http://dx.doi.org/10.5139/IJASS.2016.17.1.64

Table 1. One-year mean of daily estimation RMS errors by the extrapolation methods and GPS broadcast message (unit=TECU)

Estimation region	5°				10°			
	BRDC	BHS	LSR	NN	BRDC	BHS	LSR	NN
North	6.99	1.20	0.40	0.32	6.88	4.39	1.27	0.98
West	9.01	1.89	0.20	0.19	9.11	5.04	0.61	0.58
South	21.70	3.94	1.27	1.00	22.97	13.43	3.65	2.78
East	8.02	1.71	0.19	0.21	8.11	4.44	0.52	0.54
Total	11.85	2.68	0.75	0.60	12.61	8.83	2.19	1.69

The error reduction by either NN or LSR is magnified in Fig. 11, which shows the daily estimation error variation at the West of 5° extrapolation area in 2014. Both the NN and LSR have a very low level of RMS error while the BHS has a high level of RMS error, even greater than the North point error. This plot proves that either the NN or LSR is efficient where the spatial ionospheric gradient is low. The estimation error at East point shows the similar results as the West point.

Figure 12 shows the daily estimation error variation at the South of 10° extrapolation area in 2014. The pattern of the error variation and relative error difference is similar to the 5° results in Fig. 8. The error magnitude is approximately twice of the 5° results.

The estimation error is computed at all 24 extrapolation points and then RMS error is computed at each point. The extrapolation points are grouped into four directions and 5°/10° area. One-year average of each group's RMS error is presented in Table 1. The broadcast model error is also presented for comparison. All three methods outperform the broadcast model and it demonstrates the usefulness of the methods. The NN yields the smallest error in both 5° and 10° area. The total error reduction by the NN over the LSR is 20% for 5° area and 23% for 10° area. The differences between LSR and NN are 0.040 m for South 5°, 0.140 m for South 10°, 0.024 m for 5° extrapolation area, and 0.080 m for 10° extrapolation area. These errors cannot be ignored depending on the applications e.g. SBAS application which acceptable error is less than 0.4 m. The South area shows the largest error among the four directions. The standard deviation of the RMS error, not shown in the table, has the largest value at the South area. Therefore, irregularity of the RMS error is most significant at the South area.

6. Conclusions

The coverage area of GNSS regional ionospheric correction model is mainly determined by the distribution of GNSS ground monitoring stations. Extending the coverage area is tested by applying extrapolation techniques. We proposed an extrapolation methodology combining two types of input data, observed TEC and environmental parameters. Three methods, BHS, LSR, and NN, are tested to evaluate the extrapolation accuracy of the ionospheric delay corrections outside the correction coverage area. IGS ionosphere map data is used to simulate the corrections and to compute the extrapolation error statistics. The observed TEC and environmental parameters are used for training the NN and for fitting the LSR. One solar cycle data, i.e. 11 years of data, is used for the training and fitting.

Among the three methods, NN method yields the best accuracy. One year average of daily RMS error is 0.60 TECU at 5° extrapolation area and 1.69 TECU at 10° extrapolation area. The LSR's accuracy level is lower than the NN but significantly better than the BHS. The BHS error level is proportional to the observed TEC level, but the NN or LSR error level shows less correlation with the observed TEC level. The estimation error is increased during Spring and Fall. The error has a large value in South and North sides. All the three methods outperform the GPS broadcast ionospheric model.

Acknowledgement

The work has been supported by the National GNSS Research Center program of Defense Acquisition Program

Administration and Agency for Defense Development.

References

[1] McKinnell, L. A. and Friedrich, M., "A neural network-based ionospheric model for the auroral zone", *Journal of Atmospheric and Solar-Terrestrial Physics*, Vol. 69, No. 12, 2007, pp. 1459–1470.

[2] Habarulema, J. B., "A contribution to TEC modelling over Southern Africa using GPS data", PhD. thesis, Rhodes University, Grahamstown, 2010.

[3] Habarulema, J. B., Lee-Anne McKinnell, L. A. and Opperman, B. D., "Regional GPS TEC modeling; Attempted spatial and temporal extrapolation of TEC using neural networks", *Journal of Geophysical Research: Space Physics (1978–2012)*, Vol. 116, No. A4, 2011, pp. 1-14.

[4] El-naggar, A. M., "Artificial neural network as a model for ionospheric TEC map to serve the single frequency receiver", *Journal of Alexandria Engineering*, Vol. 52, No. 3, 2013, pp. 425-432.

[5] Wielgosz, P., Grejner-Brzezinska, D. and Kashani, I., "Regional Ionosphere Mapping with Kriging and Multiquadric Methods", *Journal of Global Positioning Systems*, Vol. 2, No. 1, 2003, pp. 48-55.

[6] Opperman, B. D., Cilliers, P. J., McKinnell, L. A. and Haggard, R., "Development of a regional GPS-based ionospheric TEC model for South Africa", *Advances in Space Research*, Vol. 39, No. 5, 2007, pp. 808-815.

[7] Kim, J. and Kim, M., "Extending ionospheric correction coverage area by using extrapolation methods", *Journal of Korean Society Aeronautics Science and Flight Operations*, Vol. 22, No. 3, 2014, pp. 74- 81.

[8] Foster, M. P. and Evans, A. N., "An evaluation of interpolation techniques for reconstructing ionospheric TEC maps", *IEEE Transactions on Geoscience and Remote Sensing*, Vol. 46, No. 7, 2008, pp. 2153-2164.

[9] Sandwell, D. T., "Biharmonic spline interpolation of GEOS-3 and SEASAT altimeter data", *Geophysical Research Letters*, Vol. 14, No. 2, 1987, pp. 139-142.

[10] Momami, S. and Odibat, Z. M., "Fractional green function for linear time-fractional inhomogeneous partial differential equations in fluid mechanics", *Journal of Applied Mathematics and Computing*, Vol. 24, No. 1, 2007, pp. 167-178.

[11] Jeff Heaton, *Introduction to neural networks with Java*, Heaton Research, Inc., 2008.

[12] Hagan, M. T., Demuth, H. B., Beale, M. H. and De Jesús, O., *Neural network design*. Boston: Pws Pub., 1996.

[13] Jwo, D. J., Lee, T. S. and Tseng, Y. W., "ARMA neural networks for prediction DGPS pseudorange correction", *Journal of Navigation*, Vol. 57, No. 2, 2004, pp. 275-286.

[14] Mohri, M., Rostamizadeh, A. and Talwalkar, A., *Foundations of machine learning*, The MIT press, 2012.

[15] Ljung, L., *System identification toolbox*, The MathWorks Inc., South Natick, MA, USA, 1988.

[16] Kim, J., Lee, S. W. and Lee, H. K., "An annual variation analysis of the ionospheric spatial gradient over a regional area for GNSS applications", *Advances in Space Research*, Vol. 54, No. 3, 2014, pp.333-341.